ISSN Print: 2394-7500
ISSN Online: 2394-5869
Impact Factor: 5.2
IJAR 2015; 1(10): 325-330
www.allresearchjournal.com
Received: 16-07-2015
Accepted: 17-08-2015

JS Dargad
Dayanand Science College,
Latur-413 531, M.S, India

Correspondence
JS Dargad
Dayanand Science College,
Latur-413 531, M.S, India

CdMnS DMS thin films: Synthesis, Structural and Transport Characteristics

JS Dargad

Abstract
$Cd_{1-x}Mn_xS$ thin films with x value ranging between 0 to 0.5 were deposited onto the glass substrates using a chemical deposition process. The composition of the as- grown samples was determined by an EDS technique. The polycrystalline growth resulted over the whole range studied and both CdS and $Cd_{1-x}Mn_xS$ films exhibited hexagonal wurtzite structure with growth orientation along (101) direction. Typically, the lattice parameter 'a' decreased from $4.131A^0$ to $4.110A^0$ for the change of x from 0 to 0.1 and thereafter it returned to its original value. Similar changes in c with x were also observed (6.710 A^0 to 6.688 A^0). Average crystallite size increased with increase in x from 0 to 0.1 and then decreased for further increase in x. The electrical conductivity is found to be enhanced with x upto 0.01 and then decreased with further increase in x. The activation energies were calculated in both the conduction regions. The transport characteristics such as thermoelectric power, carrier concentration (n), mobility (μ), and barrier height (Φ_b) were studied as a function of the working temperature and materials composition and attempted to correlate with the observed changes in structural characteristics.

Keywords: SMS, Chemical growth process, Mn^{2+} magnetic ions, spin-spin exchange, lattice parameters

1. Introduction
Recently, the semi magnetic semiconductors (SMS) in ternary and or quaternary alloyed forms are of immense importance because their fundamental semiconding properties (such as the band gap, the carrier effective mass and mobility, etc.) can be varied under smooth control of the molar composition as in the non-magnetic counterpart and that they exhibit magnetic properties as disordered magnetic alloy [1-7]. The other most important features of these materials originated in the presence of substitutional magnetic ions which leads among other things, to spin – spin exchange interactions between the localised magnetic moments of the magnetic ions and the band electrons [1-7]. This in turn impacts on the band structure and impurity states, leading to quite new effects in, e.g. magneto-optics and carrier transport, particularly when quantizing magnetic field is present [2]. Furthermore, the rich spectrum of new physical phenomena ascribed to SMS singularities hold promise for new device applications such as in IR- detectors, optical non-reciprocal devices and tunable Raman spin-flip lasers. These materials are mainly prepared by combining the magnetic ions such as Mn, Fe, Co, etc with the chalcogenides of cadmium, mercury, lead and zinc [1-11] and their high optical absorbances and nearly matching bandgaps in the visible and near IR regions of the electromagnetic spectrum are the basic characteristics for their popularity. Among these materials, CdS has an important place because of its major contribution in the photovoltaic detectors, light amplifiers, electro photography, light emitting diodes, etc. [2, 4, 5, 8, 11, 12]. It can be synthesized with ease and without any sophisticated instrumentation and can be alloyed very easily that results in the composition dependent scenario of the materials properties changing smoothly by controlling the system parameters [2, 4, 8, 13-20].
In the early stages of SMS development, it was the II – VI compound semiconductors containing substitutional Mn^{+2} ions which received major attention and consequently these are the most common and thoroughly studied SMS [1-5, 13-16]. The most studied SMSs are A^{II} Mn_x B^{VI} (where A = Zn, Cd, Hg, and B = S, Se, Te) alloys and are direct gap semiconductors [2, 4, 8, 14-12]. (Cd, Mn), (Zn, Mn), and (Hg, Mn) chalcogenide mixed crystals are typical and the most extensively studied SMS. Their remarkable physical properties are characterised by

the combination of usual semiconductor mixed – crystal behaviour with the special properties caused by the half – filled *3d* – shell of the Mn^{+2} cations. For both the basic and application reasons there is a continuous growing interest, which has been further stimulated by the preparation of quantum well structures and superlattices on the basis of these materials [2, 5, 14, 17]. Among these, $Cd_{1-x}Mn_xS$ is a distinguishable SMS from others because it has a $p - d$ exchange integral value considerably large that causes various abnormal phenomena experimentally observed [18-20]. Because of the half – filled *3d* shell, manganese (hybridization of large mole content) can contribute to the *s – p3* bonding and can substitutionally replace Cd atoms in CdS by forming a solid solution and allowing the possibilities of tailoring its properties [18-20].

2. Experimental procedure

2.1. Materials synthesis

CdS and $Cd_{1-x}Mn_xS$ thin layers of various x values ($0 \leq x \leq 0.5$) were deposited onto the mechanically cleaned glasses by a solution growth technique [4, 8, 20, 21]. Hydrolyzed solutions of cadmium sulphate (1M), manganese sulphate (1M), and thiourea (1M) in their stoichiometric proportion were taken in a glass beaker 250 ml in capacity. Triethanolamine (TEA) and liquid ammonia (NH_3) were added into the reaction container as the complexing agents. For each of the deposition, the film stoichiometry was maintained by adjusting the ion concentration volumes of the basic reactants. The glass substrates were cleaned and mounted on a specially designed substrate holder and were rotated in the reaction mixture by means of a constant speed gear motor. This provides a continuous and uniform mechanical churning of the reaction mixture. To obtain good quality samples, the amount of complexing agent, the deposition time, temperature, pH and speed of the substrate rotation were optimized [21-23].

2.2 Experimental tools and techniques

Chemical composition of the films was determined using a KEVEX-7000-77 ED spectrometer. The accelerating voltage was 20kV.

The structure and crystallinity of all the samples were examined by an X-ray diffraction technique. A Philips- PW 3710, X- ray diffractometer (with CuK_α line, $\lambda = 1.5406\ A^0$) was used for this purpose. The range of 2θ angles was from 20^0 to 80^0. The X-ray diffractograms were further analyzed to determine the crystal structure, lattice constants, crystal orientation and crystallite size.

The dc electrical conductivities of all the samples were measured by a four probe conductivity measuring unit. Silver paint was applied to the samples for ohmic contact purpose. A regulated dc power supply (Aplab make) was used to pass the current through the sample. The potential drop across the sample was measured with a HIL - 2665, 4, 1/2 digit multimeter and current through the sample was detected by a DNM - 121, 4, 1/2 digit nanoammeter. A chromel- alumel thermocouple was used to sense the working temperature. The range of working temperature was from 300 K to 600 K.

The thermoelectric power measurements were carried out on these samples in the 300-550 K temperature range. A Hewlett - Packard, 6, 1/2 digit multimeter was used to measure the thermovoltage. The gredient of temperature was measured with a Cr-Al thermocouple. Silver paint was applied to the sample for ohmic contact purpose.

3. Results and discussion

The $Cd_{1-x}Mn_xS$ ($0 \leq x \leq 0.5$) thin films were analyzed by an energy dispersive spectroscopy technique (EDS). The film constituents Cd^{2+}, Mn^{2+} and S^{2-} for various film structures were determined and are listed in table.1. The as-grown CdS films are almost stoichiometric and an addition of Mn^{2+} in CdS substitutes Cd^{2+}, whereas S^{2-} content is practically remained constant. It is seen that content of Cd^{2+} decreased with increasing Mn^{2+} content in the film [20-22]. The X-ray diffractograms were therefore obtained for the as- grown CdS and $Cd_{1-x}Mn_xS$ thin film samples in the 2θ range from 20^o to 80^o to obtain the crystallographic in formations. Eight representative diffractograms are shown in fig.1. The diffractograms clearly showed that the as-deposited films are polycrystalline in nature. The analysis of these diffractograms was done and the corresponding data [the interplanar distances (d), relative intensities of reflections (I/I_{max}), hkl planes, lattice parameters (a & c) etc] were determined. It has been seen that as-deposited CdS exhibited hexagonal wurtzite structure [21-25]. There are five prominent reflections at the d-values equal to 3.346 A^0, 3.060 A^0, 2.452 A^0, 2.060 A^0, and 1.763 A^0 that correspond to the (002), (101), (102), (110), and (112) reflections, respectively. It has also been seen that the above major peaks shift towards lower 2θ side and the shift is continuous upto x = 0.1. Above x = 0.1 the changes in d-values are insignificant and tend to more or less original values of the host material. This is the indication that $Cd_{1-x}Mn_xS$ films are hexagonal wurtzite in structure [23-26]. The results are analogous to the reports of Jain [14], Cook et. al. [26], and Wiedermeir *et al* [27]. As far as the intensities of reflections for these peaks are considered, the reflected intensity (I/Imax) is highest for the strongest peak that corresponds to the (101) plane; more or less remained constant upto x = 0.1 and then decreased a little for higher x values. The variations in reflected intensities for (002), (102), (110), and (112) planes are also significant but not systematic [20, 22]. In addition to the hexagonal phases, (200) and (400) cubic phases have also been detected. Their intensities and d variations are unsystematic. The separate phases of MnS have also been detected at higher values of x. The corresponding lattice parameters of these films structures were determined. Typically, the lattice parameter a decreased from 4.131 A^0 to 4.110A^0 for the change of x from 0 to 0.1 and thereafter it remained more or less constant. Similar changes in c with x have also been observed (6.710 A^0 to 6.688 A^0) [26]. The ratio, c/a is almost constant in the range of interest. We found a close consonance with the results reported by the earlier investigators [28-32]. The decrease in lattice constant is due to the smaller atomic size of Mn than the Cd [22, 28]. A linear behaviour of both a and c with Mn^{+2} concentration (fig.2.), which follows Vegard's law, has been observed [2, 20, 22]. Note that for strained films, we expect lattice distortion due to the stress between the substrate and the film. Therefore a slight variation from the straight line behaviour might be observed. This describes the dependence of lattice constants on Mn^{2+} concentration of the bulk crystal systems. However, fig.2 shows a linear dependence of the lattice constants on Mn-concentration for the films under study which is consistence with that of the bulk crystals within the experimental error limit. Since the thicknesses of all the $Cd_{1-x}Mn_xS$ thin films under study were about 350 nm, the results indicated that the strain between the substrates and the films was released for the films having a thickness of approximately 350 nm. Hence, for all the films

in this study, the dependence of lattice constants on Mn^{2+} concentration follows that of the bulk crystal. This type of behaviour has been reported for $Cd_{1-x}Mn_xS$ thin films by Tsai *et al* [28]. Thus addition of Mn^{2+} in CdS showed formation of solid solution upto x = 0.1. The incorporation of further Mn^{2+} (x > 0.1) resulted in the formation of separate phases of both CdS and MnS [20, 22]. The average crystallite size enhanced from 200 nm to 370 nm for the increase of x from 0 to 0.1. The crystallite size decreased for further increase in x. A plot showing grain size versus the concentration is shown in fig.3. The enhancement in grain size can be co-related, at this moment, to the observed decrease in the bandgap. The decrease in grain size beyond x = 0.1can be corroborated by the XRD observations [20, 22]. As the Mn^{+2} concentration is increased, the diffraction peaks of the XRD spectra becomes broader due to reduction in the grain size [20, 22, 28]. It is recalled that the perfect infinite crystal should have an XRD peak with δ-function shape [28]. Note that the other reason for broadening in the XRD spectra might be the increase in chemical disorder as x is increased [28]. The reason that the grain size decreases as x increases can be understood as follows: A stable crystal structure of CdS (wrutzite) differs from that of MnS (rock salt). As the composition x of the $(CdS)_{1-x}$ $(MnS)_x$ solid solution increases, internal strain arises due to the structural and chemical disorder and consequently results in an unstable CdMnS solid solution. In order to stabilize the crystal structure, the grain size is reduced to release the strain as the Mn^{+2} concentrations becomes larger [28]. The electrical conductivities of all the polycrystalline CdS and $Cd_{1-x}Mn_xS$ thin film structures were measured in the 300K-600K temperature range. The measurements showed increase in electrical conductivity with increase in the working temperature. This indicates semiconducting nature of the material. The activation energies were determined for both high and low temperature regions and are cited in table.2. The conductivity activation energies in both intrinsic and extrinsic conduction regions were calculated and listed in table.2. The donor levels are produced below the bottom of the conduction band with $E_d = 2E_{a\sigma}$. The E_d's are also listed in table.2. As far as dependence of room temperature electrical conductivity on Mn^{+2} concentration is considered, it is found that the room temperature electrical conductivity has been enhanced with composition upto x = 0.01. For further increase in x, room temperature electrical conductivity decreased. This is shown in fig.4. The conductivity modulation by incorporation of Mn^{2+} in CdS lattice can be supported as follows [20, 22]: The conductivity versus film composition (σ vs x) spectrum can be understood qualitatively on the basis of the following facts: First, the deposition of Cd^{2+} and Mn^{2+} is simultaneous and hence incorporation of Mn^{2+} in CdS has two possibilities; the substitution of a divalent Cd^{2+} by a divalent Mn^{2+} and the possibility of forming Cd vacancies. Since Cd^{2+} and Mn^{2+} are codeposited, the possibility of forming Cd-vacancies can be ruled out and the only predominant mechanism is the substitution of Cd^{2+} by Mn^{2+} [20, 22, 33-38]. The compositional analysis (EDS) of CdS and CdMnS films also supported these observations [20, 33]. As the Mn - concentration in bath was increased, the film (Mn) content also increased. Further, substitution of Cd^{2+} by Mn^{2+} atoms is easily possible since the Mn^{2+} has a smaller atomic/$_{ionic}$ radius ($^{117}/_{80}$ pm) than that of the Cd^{2+} ($^{154}/_{97}$ pm) and that Mn is more electronegative (1.6 eV) than Cd (1.5 eV). This may generate donor levels in the bandgap of CdS and as Mn-content is increased these levels increase and finally merge into the conduction band and consequently conductivity increases upto x = 0.01. Also due to the fact that Mn has a smaller size and replacement of Cd^{2+} by Mn^{2+} is easily achieved; there is almost no strain induced on the lattice, especially at low concentrations of Mn in CdS. However the possibility that a small or tolerable amount of lattice strain may exists due to bond braking and making during substitution and that not all the Mn^{2+} atoms find their position in the CdS lattice cannot be ruled out. This has been reflected in the variation of σ with x and that σ increased significantly with x almost linearly and monotonically. Second, enhancement in electrical conductivity can also be partly justified by the decreased band gap in this region (i.e. upto x = 0.01). On the other hand, at higher Mn^{2+}-concentration, the decrease in electrical conductivity with x can be explained as follows. The deposition of Cd^{2+}, Mn^{2+}, and S^{2-} is simultaneous and the rate of substitution of Cd^{2+} by Mn^{2+} was initially higher and went on decreasing as the time passes and finally it becomes practically zero. At such higher level of concentrations where there is no substitution, it is likely that Mn^{2+} (so also already displaced Cd^{2+}) may adjusts themselves at the interstitial sites rather than the substitutional causing increased charge trapping centers thereby increasing the intergrain barrier potential that increases the carrier scattering reducing the electrical conduction [20, 22, 33]. Again the decrease in σ at high x values can be attributed to the increased strain on the lattice (direct consequence of which is decrease in crystallite size by releasing the strain) and an increase in the bandgap due to highly distorted lattice and that it will be under more and more increasing strain tending towards amorphosity of the material that causes band gap to increase [2, 14, 20, 22, 33]. Our XRD studies throw light on theses observations [20, 33]. The σ – x behaviour can also be explained on the basis of earlier structural observations [20, 22, 33]. The thermoelectric power (TEP) for CdS and $Cd_{1-x}Mn_xS$ thin films showed n- type conduction. The thermo electric power increased with increase in temperature, and this behaviour confirms that the electrons make the major contribution to the conductivity. The temperature dependence of thermoelectric power is initially almost linear and then tends to be a quasilinear showing degeneracy of the sample [20, 22, 33, 34]. The thermoelectric power increased with an increase in composition upto x = 0.01 and thereafter decreased above x = 0.01. The carrier densities (n) and the carrier mobilities (μ) at various temperatures were determined for all these samples. Fig.5 is a plot of the carrier concentration and mobility as a function of the composition x. It is seen that carrier concentration and mobility varied with the working temperature and the film composition; the variation in carrier mobility being significant compared with the carrier concentration. This is an indication of the scattering mechanism associated with the intercrystalline barrier potential. The temperature dependence of carrier mobility was then analyzed to evaluate the grain barrier potential by applying the Petritz's grain boundary scattering model [20, 22, 33, 36]. The calculated values of the intergrain barrier potentials (ϕ_B's) are listed in table.2, It is seen that the intergrain barrier potential decreased up to x = 0.01 and then increased for higher values of x [20, 33], a behaviour analogous to electrical conductivity.

4. Conclusions

Among the different methods available to deposit CdS and $Cd_{1-x}Mn_xS$ thin films, chemical bath deposition (CBD) must be ranked conceptually the simplest. The polycrystalline growth of thin films over the whole range studied is possible. Both CdS and $Cd_{1-x}Mn_xS$ films exhibited hexagonal wurtzite structure with growth orientation along (101) direction. The grain sizes were of the order of few hundred nm. The variation in lattice parameters showed Vegards behaviour and is an indicative of the formation of solid solution. High temperature electrical conductivity is governed by a grain boundary scattering limited conduction mechanism, whereas low temperature electrical conduction is of the variable range hopping type. The thermoelectric power is of the order of few micro volts and samples showed n- type conduction. The carrier concentration and mobility are influenced by both film composition and the working temperature.

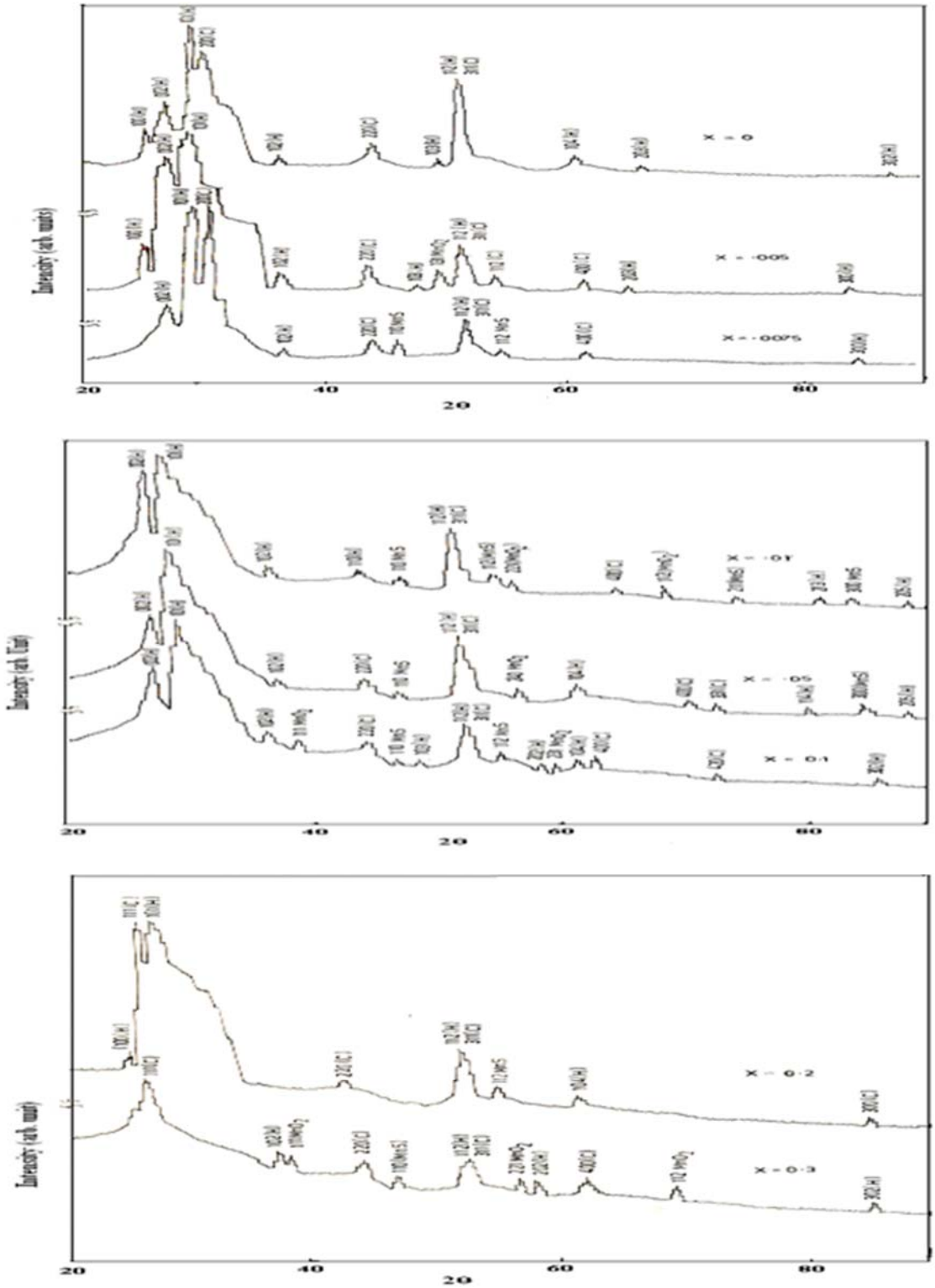

Fig.1: The X-ray diffractograms of the Cd_{1-x} Mn_xS composite structures.

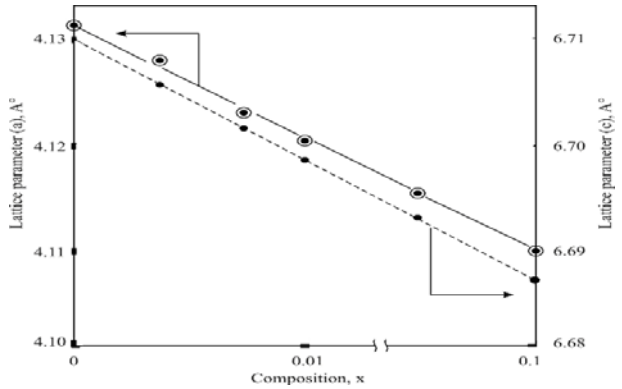

Fig 2: Variation of lattice parameters a and c with the composition. x for the solid solution region (Vegard's law obeyed).

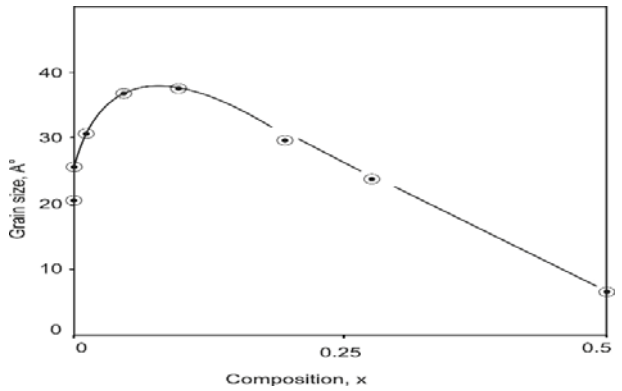

Fig 3: Variation in the crystallite size with composition x of the $Cd_{1-x}Mn_xS$ thin films ($0 \leq x \leq 0.5$).

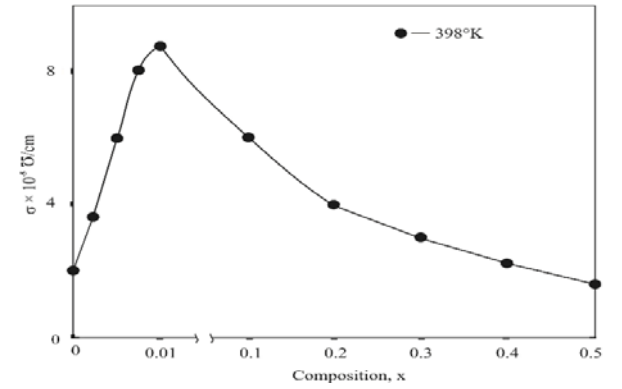

Fig 4: Variation of an electrical conductivity with the film composition x.

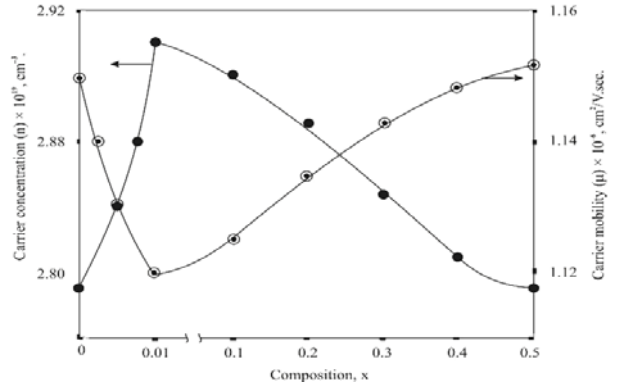

Fig 5: Dependence of carrier concentration (n) and mobility (μ) on the film composition x.

Table 1: Chemical compositional analysis of the $Cd_{1-x}Mn_xS$ thin composite films (Non destructive EDS analysis).

Composition (x)	Mn (LA) AT%	Cd (L A) AT %	S (L A) AT %
0.0	----	50.08	49.92
0.005	0.16	49.89	49.95
0.0075	0.30	49.68	50.02
0.01	1.75	48.26	49.99
0.05	2.72	47.34	49.94
0.1	3.68	46.29	50.03
0.2	5.33	41.74	49.93
0.3	8.27	41.82	49.91

Table 2: Some characteristics of the CdS and $Cd_{1-x}Mn_xS$ ($0 \leq x \leq 0.5$) thin composite films.

Composition, (x)	Acivation energy, eV		Barrier height, (ϕ_B) eV	Donor levels, E_d, eV
	$E_{a\sigma 1}$ H.T.	$E_{a\sigma 2}$ L.T.		
0.0	0.721	0.425	0.671	0.850
0.0075	0.711	0.412	0.662	0.824
0.005	0.685	0.391	0.643	0.782
0.01	0.670	0.372	0.625	0.744
0.05	0.679	0.379	0.625	0.758
0.1	0.689	0.382	0.635	0.764
0.2	0.715	0.421	0.663	0.842
0.3	0.735	0.453	0.694	0.906
0.5	0.765	0.482	0.721	0.964

5. References

1. JK Furdyna, J Appl. Phys. 1982; 53:7637
2. JM Pawlikowski. in Diluted Magnetic Semiconductor, World Scientific Publishing Com. Pvt. Lt. Singapore, 1991, 527
3. JK Furdyna, J Appl Phys. 1988; 4:64.
4. VS Karande, SH Mane, VB Pujari, LP Deshmukh. Material Letters, 2005; 59:148
5. SK Kmilla, S Basu, Bull. Mater. Sci., 2002; 543:25
6. H Nojiri, M Motokawa, S Takeyama, T Sato. Cryst J Growth, 2000; 314(215):424
7. Y Yasuda, DM Duc, Y Segawa, J Cryst. Growth, 2000; 214:159
8. VS Karande, SH Mane, VB Pujari, LP Deshmukh, J. Mat. Sci.: Mat. In Elect. 2004; 15:419.
9. GA Prinz. Science, 1990; 250:1092.
10. M Tanaka, J Vac. Sci. Technol., 1998; B16:2267
11. T Mizokawa, T Namba, A Fujimori, T Fukumora, M Kawasaki. Phys. Rev. 2002; B-65:085209.
12. A Meskauskar, J Visvakas. Thin Solid Films. 1976; 36:81
13. AK Rautri, R Thangraj, AK Sharma, BB Tripathi, OP Agnihotri. Thin Solid Films. 1982; 91:55.
14. M Jain. in Diluted Magnetic Semiconductors, World Scientific Publishing Com. Pvt. Lt. Singapore 1991.
15. AK Ramdas. J. Appl. Phys., 1982; 53:7649.
16. R Triboulet, D Didier, J Cryst. Growth. 1981; 52:614.
17. J Macovet, Optoelect. & Adva. Mat. 2006; 8:1.
18. A Twardowski, Chi. J. Phys., 1995; 33:4.
19. CT Tsai, SH Chain, DS Chu, WC Choue. Phys. Rev. 1996; B54:11555.
20. JS Dargad, EU Masumdar, LP Deshmukh, Proc. Int. Conf. on Meterological Coat. & Thin Films, San Diago, USA, 28 April-6 May, 2008.
21. JS Dargad, VS Karande, LP Deshmukh. Nat. Conf. on Semiconductor Material & Technology (NCSMT),

Gurukul Kangri Vishwavidyalaya, Haridwar, Uttarkhand, India, 2008, 16-18 Oct.
22. JS Dargad, SA Lendave, LP Deshmukh. Nat. Conf. on Recent Trends in Thin film tehnology (RTTFT-08), Walchand College of Arts & Science, Solapur, MS, India, 2008, 14-15 Nov.
23. Dana's System of Mineralogy, 7th Ed., 1, Nat. Bur. Stand. (U.S.), Circ. 539, 15. JCPD-06-0314.
24. Troemel ML, M Institut. Fűr Anorganische. Chemi, Frankfurt. West Germany, ICDD Grant-in-Aid. –JCPD-1989, 40-1289.
25. Dana's System of Mineralogy, 7th Ed., 1, Nat. Bur. Stand. (U.S.). Circ., 15, 539 JCPD-07-0222.
26. Cook Jr WC, J. Am. Ceram. Soc. 1968; 51:518.
27. H Wiedermeir, AG Sigai, J. Chem. Thermodyna. 1970; 6:981
28. CT Tsai, SH Chain, DS Chu, WC Choue, Phys. Rev., 1996; B-54:11555.
29. DS Chuu, YC Chang, CY Hsieh. Thin Solid Films, 1997; 304:28.
30. Iocami F, Salaoru I, Apetroaet N, Vasile A. Teodorescu CM, Macovet D, J Optoele. Advanc. Mate, 2006; 8:266.
31. CW Na, DS Han, DS Kim, YJ Kang, JY Lee, J Park, J. Phys. Chem., 2006; B110:6699.
32. C Chain, M Qu W Hu, X Zhang, F Lin, H Hu, Ma K, J Appl Phys. 1991; 69:6114.
33. JS Dargad. Ph.D. Thesis, SRTM University, Nanded, India, 2009.
34. GS Shahane, BM More, LP Deshmukh. Mat. Chem. Phys., 1997; 47:263.
35. LP Deshmukh, SG Hollikatti, BM More, Bull. Mat. Sci., 1994; 17:455.
36. SH Mane. Ph.D. Thesis, Shivaji University, Kolhapur, M. S. India, 2006.
37. LP Deshmukh, SG Hollikatti, BM More, Mat. Chem. Phys., 1995; 39:278.
38. GS Shahane, LP Deshmukh. Mat. Chem. Phys., 1997; 51:246.